Ionization-site effects on the photofragmentation of chloro- and bromoacetic acid molecules

Helena Levola,[1] Eero Itälä,[1] Kim Schlesier,[1] Kuno Kooser,[1] Sanna Laine,[1] Joakim Laksman,[2] Dang Trinh Ha,[1] Elisabeth Rachlew,[3] Marta Tarkanovskaja,[4] Katrin Tanzer,[5] and Edwin Kukk[1]

[1]*Department of Physics and Astronomy, University of Turku, FIN-20014 Turku, Finland*

[2]*MAX Laboratory, Lund University, Box 118, SE-22100 Lund, Sweden*

[3]*Physics Department, Royal Institute of Technology KTH, S-10691 Stockholm, Sweden*

[4]*Department of Physics, Tartu University, EST-5041 Tartu, Estonia*

[5]*Institut für Ionenphysik und Angewandte Physik, Center of Molecular Biosciences, Leopold Franzens Universität Innsbruck, 6020 Innsbruck, Austria*

(Received 25 September 2015; published 10 December 2015)

Fragmentation of gas-phase chloro- and bromoacetic acid samples, particularly its dependency on the atomic site of the initial core ionization, was studied in photoelectron-photoion-photoion coincidence (PEPIPICO) measurements. The fragmentation was investigated after ionizing carbon 1*s* and bromine 3*d* or chlorine 2*p* core orbitals. It was observed that the samples had many similar fragmentation pathways and that their relative weights depended strongly on the initial ionization site. Additional Auger PEPIPICO measurements revealed a clear dependence of fragment pair intensities on the kinetic energy of the emitted Auger electrons. The modeled and measured Auger electron spectra indicated that the average internal energy of the molecule was larger following the carbon 1*s* core-hole decay than after the decay of the halogen core hole. This difference in the internal energies was found to be the source of the site-dependent photofragmentation behavior.

DOI: 10.1103/PhysRevA.92.063409 PACS number(s): 33.80.Gj

I. INTRODUCTION

Much has been learned in recent decades about the photoinduced molecular dynamics and dissociation of free molecules owing to the availability of powerful and tunable x-ray and ultraviolet radiation sources—synchrotrons [1–13]. The ability to tune the photon energy to the desired resonance or above or below a certain absorption edge allows observing the molecule's response to photon absorption in great detail and provides a means to manipulate this response. In broad terms, the triggering events of photoionization and dissociation can be divided into three main categories: (i) valence ionization, (ii) core-level ionization, and (iii) core-level resonant excitation. Each category produces specific features in the ensuing fragmentation dynamics. Synchrotron radiation enables one to selectively reach atomic inner shells, promoting electrons to either bound (resonant excitation) or continuum orbitals. In both cases, it is possible to select and/or determine exactly which atomic site in the molecule absorbs the energy by virtue of either choosing a suitable resonant energy or measuring the emitted photoelectron's energy. This has acted as the motivation for many studies on the ionization site-dependent properties of molecular photodissociation.

Numerous such studies have concentrated on the resonant core-excitation processes [1,3–5,7–9,12–19], starting from the pioneering works of Eberhard *et al.* [1] and Nenner *et al.* [3]. Here, the core-excited state, albeit short lived, plays a crucial role in initiating the fragmentation dynamics since by core excitation an electron can be placed in a previously vacant molecular orbital with strong antibonding properties. In contrast, the *core-ionized* intermediate state retains much of the bonding character of the neutral ground state since the removal of a core electron has no direct effect on the bonding orbitals (see, e.g., Ref. [20]). Thus, the core-ionized states are typically bound, although some geometry changes may take place. The second crucial difference is that the Auger decay, predominantly following either the core excitation or the ionization in the soft x-ray range, creates mostly singly ionized parent molecules in the first but doubly ionized ones in the second case. The subsequent dynamics is strongly influenced by the Coulomb repulsion between the charged fragments in the latter. Despite such fundamental differences, the related literature is sometimes unclear or misleading in relation to whether a resonant or nonresonant site dependency is discussed.

The site-dependent effects in photoexcitation can be very strong and related to the specific properties of a particular resonant intermediate state [8]. In contrast, such effects following core ionization are often less pronounced [9,11,21,22] or are sometimes not observed at all [23,24], although in several cases strong site dependency has also been observed [5,6,10,16,18,25–31]. In light of the increasing interest in photodissociation in biologically relevant molecules and in radiation damage at the molecular level, such processes are highly relevant since an x-ray exposure event predominantly results in a core ionization, instead of a resonant core-excitation process. Here, we concentrate on site-dependent fragmentation of core-ionized carbon or halogen atoms in the bromo- and chloroacetic acid molecules and discuss the physical foundations of this effect.

In core ionization, site dependency has been observed, e.g., in an ozone molecule [10] where the $O^+/O_2{}^+$ branching ratio varied depending on the terminal vs central oxygen ionization and on the vibrational levels in the core-ionized intermediate state. The authors conclude: "*The observed bond break selectivity is probably a result of two distinct processes; population of different final states dependent on the core-hole state and nuclear motion before Auger decay.*" Another triatomic molecule where site-dependent fragmentation in core ionization has been observed is CO_2 [31]. Eland *et al.* briefly discussed site-selective photochemistry on the example of acetone and stated: "*. . . by far the most important factor determining the outcome of molecular fragmentation is the amount of energy deposited in the molecule or ion . . .*" [27]. This conclusion

is in line with an earlier study of bromochloromethane by Miron *et al.* [6], who observed a strong preference for the photodissociation to cut the bond to the particular halide atom (Cl or Br) that was core ionized. This site dependency, however, was observed only for low internal energies of the doubly charged ion. In a recent study of a medium-sized molecule thiophene [32], the internal energy was observed to have a great influence on the fragmentation, although this study did not specifically concern site-dependent effects. Among larger molecules, site-dependent effects were observed in the fragmentation of the $F_3SiCH_2CH_2Si(CH_3)_3$ molecules by Nagaoka and co-workers [25,26] as the two silicon atoms were core ionized and distinguished by means of the chemical shifts in the $2p$ photoelectron energy. In Ref. [25] the authors take a somewhat different viewpoint from the work in Refs. [10] and [27], postulating that "*Since these* [created by the normal Auger decay] *valence holes weaken chemical bonds around the initially core-ionized atom, site-specific fragmentation . . . often occurs around it.*" Later, the study was extended to other molecules with varying hydrocarbon chains between the Si-containing end groups, and the strength of the site-dependent effect was seen to correlate with the chain length [26].

Thus in core ionization, a number of physical reasons have been thought to be responsible for the site-dependent fragmentation behavior. It has also become apparent that the exact mechanisms translating the site-specific ionization into various fragmentation patterns as the events of core ionization, Auger decay, and bond dissociation proceed remain an open question which is targeted in this paper.

Experimentwise, the various multiparticle coincidence methods have proven to be excellent tools for studying site-dependent molecular fragmentation [2,4–11,16–19,21–30,33,34]. Specifically, the electron-energy-resolved photoelectron-photoion-photoion coincidence (PEPIPICO) method was also employed in the present study. In PEPIPICO, by detecting the emitted photoelectron of specific energy in coincidence with the ionic fragments, it is possible to record a fragmentation pattern following the core ionization of different atomic sites, even of the same element as long as the photoelectrons are energy separated by chemical shifts exceeding the electron energy resolution.

In a PEPIPICO measurement, the Auger electron and photoelectron are not detected in coincidence, which in general means that the information about the final states of the Auger decay is not obtained in the same measurement as the site-specific information. However, it is often possible to retain the information on the initial core-ionization site in the energy-resolved Auger electron-ion-ion coincidence measurement (sometimes referred to as AEPIPICO) since vacancies in different elements and core orbitals result in the Auger spectra in different energy ranges. In the present study, PEPIPICO experiments were complemented by the AEPIPICO results.

The principal constituents of organic molecules, i.e., carbon, oxygen, nitrogen, and hydrogen atoms, each contribute to the molecular orbitals which tend to be delocalized over a large region of the molecule. However, the valence electrons of a substitute halogen element, for example, combine with the rest of the molecule more selectively, often creating much more localized orbitals. This localization also makes the Auger decay and its final-state population sensitive to the location of the initial core hole. In consequence, the halogen-substituted molecules have become a popular subject of research [5,6,8,9,11,16–19,21,25–28,34]. Moreover, with multiple halogen substituents within one molecule, it is possible to create the initial core holes in otherwise indistinguishable environments and investigate the effect of the geometrical or chemical location of the initial ionization site with only one sample [18]. The halogenated samples used in this study are depicted in Fig. 1.

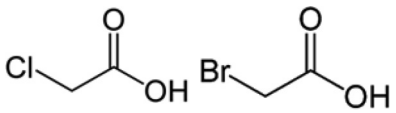

FIG. 1. Chloroacetic acid (left) and bromoacetic acid (right).

II. EXPERIMENTAL SETUP AND TECHNIQUES

The site-dependent fragmentation of gas-phase chloroacetic acid (ClAA) and bromoacetic acid (BrAA) samples was studied by combining information from different experiments. PEPIPICO measurements were performed in order to examine the differences in fragmentation after ionizing carbon $1s$ and Cl $2p$ or Br $3d$ core orbitals. In order to elaborate on the role of internal energy, additional AEPIPICO measurements were performed for ClAA in which mass spectra were collected in coincidence with Auger electrons emitted after Cl $2p$ core hole decay. Two different electron spectrometers were used in these experiments. During the PEPIPICO measurements of ClAA, kinetic energies of the photoelectrons were analyzed with a modified Scienta SES-100 analyzer where the original CCD camera was replaced with a resistive anode detector by Quantar. In all other experiments, the electron analyzer was a modified Omicron EA-125 where again a resistive anode detector [Quantar, 40-mm active area microchannel plate (MCP)] was used instead of the original channeltron detector. The supplier's acquisition control software, power supplies, and lens optimization settings were also replaced by self-developed ones that were specifically optimized for coincidence experiments. Details about the measurement settings in different experiments are provided in Table I.

In all measurements, the coincident ions were detected with a homemade Wiley-McLaren-type time-of-flight (TOF) mass spectrometer with a 77-mm Hamamatsu MCP detector. The ion spectrometer was operated in pulsed extraction mode. The samples with stated purities of 99% for ClAA and 97% for BrAA were purchased from Sigma-Aldrich and used without further purification. No heating was required for sample evaporation.

The coincidence measurements were triggered by the detection pulse from the preamplifier of the electron detector. The data collected from the pulsed extraction mode coincidence measurements inevitably contain false ion-ion or ion-electron coincidences that do not originate from the same ionization event. To minimize the fraction of these false coincidences, low counting rates, typically less than 20 electrons s, were used in all measurements. In addition to the electron triggered

TABLE I. Experimental details for the coincidence measurements of ClAA and BrAA samples and for noncoincident electron spectra (Auger) of ClAA.

Measurement-sample	Ionization site	Photon energy (eV)	E_{pass} (eV)	Kinetic-energy range (eV)	Entrance slit width (mm)	Energy resolution (eV)
PEPIPICO-ClAA	C 1*s*	325	100	25–44	1.6	0.8
	Cl 2*p*	240	100	28–36	1.6	0.8
PEPIPICO-BrAA	Cl 1*s*	315	50	18–26	6	1.4
	Br 3*d*	95	100	15–28	6	2.4
AEPIPICO-ClAA	Cl 2*p*	250	200	155–182	6	4.8
Auger-ClAA	Cl 2*p*	250	50	140–180	1	0.25
	C 1*s*	320	50	230–270	6	1.4

data, another set of coincidence data triggered by a pulse generator at fixed frequency was collected. This "artificially" triggered dataset was used to statistically reduce the influence of false coincidences in the final analysis. A more detailed description of the coincidence setup and technique can be found in Ref. [35].

In addition to the coincidence measurements, Auger electron spectra of ClAA were collected in a regular scanning acquisition mode of the spectrometer. The details of these measurements are also provided in Table I.

The experiments were performed at the undulator beamline I411 of the MAX II Laboratory in Sweden [36]. The spectrometers were mounted perpendicular to the light propagation with the electron analyzer angle of detection 0° to the polarization vector of horizontal linearly polarized light. The radiation was monochromatized with a Zeiss SX-700 plane-grating monochromator.

III. RESULTS AND DISCUSSION

A. Fragment pair identification

The emphasis of this paper is on the site-dependent effects of the fragmentation and not on the details of the various fragmentation channels themselves. In addition, in some cases it is impossible to deduce the exact dissociation sequences of the observed fragment pairs from the PEPIPICO data. For these reasons, we only address the fragmentation behavior of the samples briefly.

The results of the PEPIPICO measurements are represented in two-dimensional maps where the flight times (masses) of the heavier and lighter coincidence ions are plotted on the *y* and *x* axes, respectively. Figure 2 shows the photoion-photoion-coincidence (PIPICO) maps of ClAA and BrAA from the halogen core-level ionization. The pairs including bromine are clearly distinguishable by the double patterns caused by the two bromine isotopes (the relative abundances are 50.7% for ^{79}Br and 49.3% for ^{81}Br). For example, the pattern of the pair marked in Fig. 2 as ($C_2OH_n^+$,BrH_m^+) consists of two narrow tilted linelike patterns displaced vertically; the lower corresponding to a pair with the heavier ion containing ^{79}Br, and the upper containing ^{81}Br. The isotope effect is also responsible for the distorted appearance of the patterns (CH_n^+,Br^+) since here the two patterns have a steeper slope and partly overlap, creating a visual effect of a single curved pattern. The isotope effect of chlorine is less evident due to very less balanced abundances of the chlorine isotopes (75.8% for ^{35}Cl and 24.2% for ^{37}Cl).

As can be seen from Fig. 2, the fragmentation of both samples is dominated by ion pairs including a halogen atom *X*. In both samples, the most intense pairs contain X^+ or XH^+, and in ClAA XCH_m^+ ($m = 0$, 1, or 2). Only a few pairs can be observed that do not contain halogen at all.

When comparing the fragment pairs of BrAA and ClAA, we have assumed that ions differing only by the number

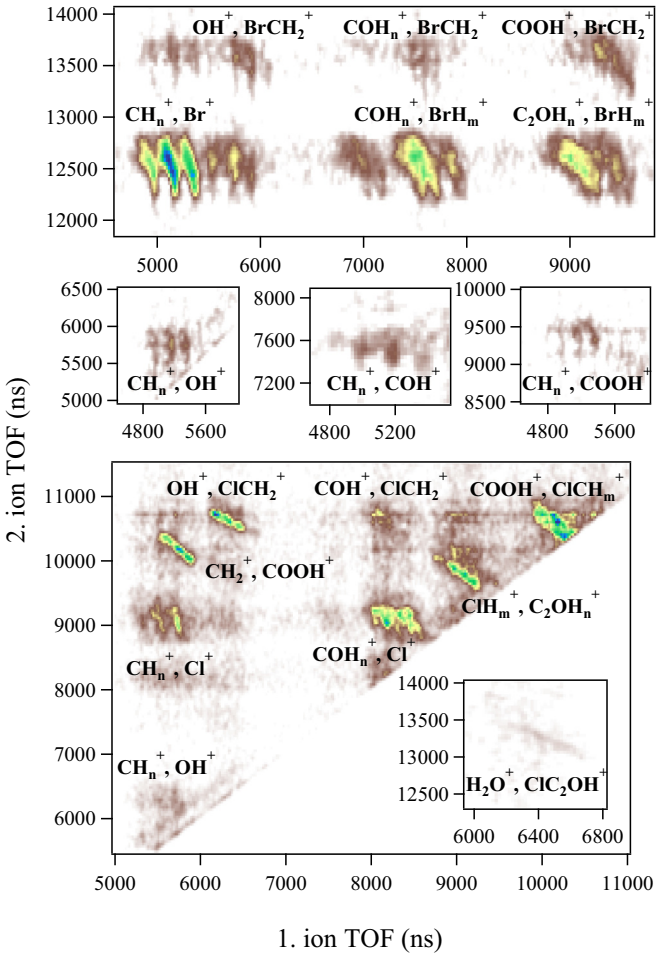

FIG. 2. (Color online) PIPICO maps of bromoacetic acid (top) and chloroacetic acid (bottom) from the halogen (Br 3*d* and Cl 2*p*) core-level ionization.

TABLE II. Common fragment pairs for bromoacetic and chloroacetic acids.

Fragment pair	n		m			
(X = Cl or Br)	ClAA	BrAA	ClAA	BrAA	Fragmentation pathway	Breaking bonds[a]
$COOH^+, XCH_m^+$			0–2	2	Two-body dissociation with possible hydrogen loss	**C-**C **C-**C
COH_n^+, XCH_2^+	1	0–1			Secondary dissociation Deferred charged separation	**C-C** and C-O C-O and **C-**C
OH^+, XCH_2^+					Secondary dissociation	**C-O** and C-C
$COOH_n^+, XH_m^+$	0	0–1	1	0–1	Secondary dissociation Secondary dissociation	**C-C** and *X*-C ***X*-C** and C-C
$C_2OH_n^+, XH_m^+$	1–3	1–2	0–1	0–1	Secondary dissociation Deferred charge separation	***X*-C** and C-O C-O and ***X*-C**
COH_n^+, XH_m^+	1	0–1	0	0–1	Secondary dissociation Secondary dissociation	**C-C**, *X*-C, and C-O ***X*-C**, C-C, and C-O
COH_3^+, X^+					Secondary dissociation Secondary dissociation	**C-C**, *X*-C, and C-O ***X*-C**, C-C, and C-O
CH_n^+, X^+	0–2	0–2			Secondary dissociation Secondary dissociation	**C-C**, *X*-C, and C-O ***X*-C** and C-C
$CH_n^+, COOH^+$	2	0–2			Deferred charge separation Secondary dissociation	*X*-C and **C-**C **C-C** and *X*-C
CH_n^+, OH^+	0–2	0–2			Secondary dissociation Secondary dissociation Secondary dissociation	**C-C**, *X*-C, and C-O *X*-C, **C-C**, and **C-**O **C-O**, *X*-C, and C-C

[a]Listed in the order of occurrence. The bonds in bold indicate the bonds across which the charge separation occurs. The bonds between hydrogens and other atoms are not considered.

of hydrogens originate from same kind of fragmentation process and have therefore considered them together, e.g., the pairs (C^+, Br^+), (CH^+, Br^+), and (CH_2^+, Br^+) are considered as one pair with the notation (CH_n^+,Br^+), and their intensities are summed in the analysis. As an exception, we have examined the pairs (COH_n^+, XH_m^+), where $n = 0$ or 1, and (COH_3^+, X^+) separately because we do not observe ions with $n = 2$. With such a classification, we have identified ten similar ion pairs for these two samples. They are listed in Table II along with the information on their fragmentation pathways. It should be noticed that the number of hydrogens in a given fragment pair can be different in different samples. The values for n and m for both samples are provided in Table II.

B. Fragmentation dynamics

Although following the dynamic sequences leading to the observed patterns is not the aim of this study, the last column of Table II also presents the bond-breaking sequences and charge separation in a stepwise dissociation model. The only pair resulting from a two-body dissociation is ($COOH_n^+, XCH_m^+$); all the other pairs originate from fragmentation processes having multiple dissociation steps.

In most cases, there are alternative pathways leading to a certain fragment pair. In order to distinguish between these, quantitative analysis of the pattern shapes is required. The exact sequence of steps affects the slope ($\Delta TOF_2/\Delta TOF_1$) of the patterns in the PEPIPICO maps as described, e.g., in Ref. [37]. For some pairs, however, the PEPIPICO patterns are too weak or blurry in order to reliably analyze their slopes. Furthermore, detailed analysis of even the strongest features in the map is hindered by: (i) the creation of double patterns due to two halogen isotopes and (ii) the variability in hydrogen dynamics also creating multiple patterns. Therefore, all viable sequences are listed in the last column of Table II in cases where several possible pattern slopes can fit within the experimental error bars. Below, some of the clearest cases on the example of ClAA are illustrated.

When the first bond to break and separate the charges is the C-O in the carboxyl group, it leads to the (OH^+, XCH_2^+) pattern. In this case, the C-C bond to the carboxyl group breaks as a secondary dissociation of the singly charged $ClCH_2CO^+$ intermediate. Such a sequence predicts a pattern with a slope less steep than -1 as indeed observed (Fig. 2). The experimental slope was found to be -0.71 ± 0.07, which fits into the proposed fragmentation sequence. This pattern also was sufficiently well defined for a kinetic-energy release (KER) analysis, which was found to be 1.1 ± 0.2 eV. Similar analysis could also be performed for the pattern of ($COOH^+$,CH_2^+) of ClAA which originates from a secondary dissociation of CH_2COOH^+ moiety after the neutral Cl loss. In this case, the KER was found to be 1.05 ± 0.2 eV. For the other patterns, KER analysis was not possible due to the low intensity or overlapping patterns.

Another case of charge separation followed by secondary fragmentations is observed in the patterns of (CH_n^+, X^+). The two possible pathways in Table II predict, for ClAA, the slopes of approximately -2.5 and -4.2. In both cases, one should observe patterns with steep slopes as in Fig. 2. Third, in the case of the pairs ($C_2OH_n^+$,ClH_m^+), the possible

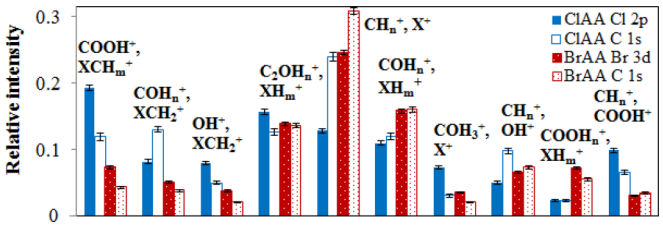

FIG. 3. (Color online) Relative intensities of common fragment pairs of ClAA and BrAA according to the initial ionization site. X refers to chlorine or bromine. Statistical error bars are shown on top of the bars.

primary dissociation processes are either rupture between the halogen and the rest of the molecule or a loss of the neutral hydroxyl group. The latter process would result in a slope of -1, whereas the former would lead to a slope less steep than -1. Both fit reasonably well into the patterns.

C. Ionization-site-dependent fragmentation

The relative intensities of each ion pair according to the sample and the ionization site are provided as a graph in Fig. 3. Only the fragment channels found in both samples are provided. Strong site-dependent effects can be observed from the graph, especially in the case of chloroacetic acid. As can be seen, the relative intensities of the pairs $(COOH^+,XCH_m{}^+)$,$(OH^+,XCH_m{}^+)$, and $(COH_3{}^+,X^+)$ are smaller in C $1s$ ionization than after halogen core-level ionization, regardless of the sample. The opposite is observed for pairs $(CH_n{}^+,X^+)$,$(COH_n{}^+,XH_m{}^+)$, and $(CH_n{}^+,OH^+)$. The smaller intensity of the pair $(COOH^+,XCH_m{}^+)$ resulting from two-body dissociation suggests increasing secondary dissociation following C $1s$ ionization. This interpretation is supported by the enhancement in the production of pairs originating from multiple step dissociation processes and especially those involving bond ruptures in more than two bonds, i.e., pairs $(COH_n{}^+,XH_m{}^+)$,$(CH_n{}^+,X^+)$, and $(CH_n{}^+,OH^+)$ (see Table II). The smaller intensities of $(COH_3{}^+,X^+)$ pairs probably reflects the enhancement in $(COH_n{}^+,XH_m{}^+)$ production by subsequent hydrogen loss. In addition, further dissociation of pairs $(OH^+,XCH_m{}^+)$ would contribute to the increase in the relative intensities of the pairs $(CH_n{}^+,OH^+)$.

The six pairs mentioned above behave similarly in both samples, but there are also differences. One example is seen in the pair $(COH_n{}^+,XCH_2{}^+)$, whose relative intensities change differently between the samples. The reason for this remains unsolved. Different behaviors can also be observed in the two rightmost fragment pairs in Fig. 3: $(CH_n{}^+,COOH^+)$ and $(COOH_n{}^+,XH_m{}^+)$. In C $1s$ ionization, the relative intensity of $(CH_n{}^+,COOH^+)$ pairs appears to be smaller than the one in the Cl $2p$ ionization in ClAA, whereas in BrAA the two relative intensities are equal within the error bars. The relative intensity of $(COOH_n{}^+,XH_m{}^+)$ pairs of BrAA declines in C $1s$ ionization, whereas in ClAA it is the same for different ionization sites. In other words, the $(CH_n{}^+,COOH^+)$ pair in ClAA has the same site-dependent behavior as the $(COOH_n{}^+,XH_m{}^+)$ pair in BrAA and, correspondingly, neither the intensity of the $(CH_n{}^+,COOH^+)$ pair in BrAA nor of the $(COOH_n{}^+,XH_m{}^+)$ in ClAA shows site dependency. This apparent disagreement disappears when one realizes that both fragment pairs represent the same breakup pattern with a different charge localization. The very clear pattern of the $(CH_2{}^+,COOH^+)$ fragment pair of ClAA (see Fig. 2) has a slope close to -1, indicating a fragmentation process where chlorine separates as a neutral fragment followed by two-body charge separation of the CH_2COOH^{++} ion. However, if the halogen atom in BrAA was separated as a charged fragment, the subsequent secondary dissociation of CH_2COOH^+ moiety would lead to the formation of $(COOH_n{}^+,XH_m{}^+)$ pairs. Such a dissociation sequence would result in a pattern with slope -1.3, which fits reasonably well in the observed pattern, although the weak pattern intensity does not allow the determination of the exact slope value. When these pairs are examined as one multistep breakup process,

$$\begin{aligned} XCH_2COOH^{2+} &\rightarrow XH_m^{(2-q)+} + CH_nCOOH^{q+} \\ &\rightarrow XH_m^{(2-q)+} + COOH^+ + CH_n^{(q-1)+}, \end{aligned}$$

the difference remains only in the charge assignment (ClAA: $q = 2$, BrAA: $q = 1$), explaining how the intensities of $(COOH_n{}^+,XH_m{}^+)$ in BrAA could behave as the intensities of $(CH_2{}^+,COOH^+)$ in ClAA. In the above, the bromine fragment is ionized, but chlorine is neutral. Based on the experiment alone, we cannot offer a complete explanation for this difference; however one should take into account that the ionization energy of chlorine is about 1.2 eV higher than that of bromine. This can at least partly go towards explaining the differences.

In addition to the comparison of the fragmentation patterns following halogen and carbon ionizations we were able to investigate the differences resulting from the ionization of the two carbon atoms C_x and $C_{carboxyl}$ since their $1s$ photoelectron peaks are separated by approximately 2.8 and 3.5 eV in ClAA and BrAA, respectively, and are resolved in the PEPIPICO photoelectron spectra. Differences in the ion-pair intensities are much smaller than in the halogen vs the combined carbon-ionization case and remain mostly within the error bars. However, a general tendency can be observed that the small changes in the fragmentation pattern resulting from the C_x $1s$ ionization, when comparing to that of $C_{carboxyl}$, are towards the pattern resulting in halogen ionization.

The results summarized by Fig. 3 clearly show significant site-dependent effects in the halogenated acetic acid molecules. In contrast with earlier studies of halogenated molecules [6,18], however, the site dependency is not as clear cut as the preferred separation of the halogen atom being core ionized. In fact, there are channels where the X-C bond is cut but that show the opposite trend: for example, the $(CH_n{}^+,Cl^+)$ patterns (and the analogs in BrAA) are strongly enhanced in the *carbon* core ionization.

D. Auger decay spectra of core vacancies—calculation

When interpreting the effects of the core-hole location on the fragmentation patterns, it must be kept in mind that the core hole is very short lived with a lifetime of several femtoseconds and, in the absence of an excited electron, has a minor effect on the molecular dynamics. Instead, the effects of the core-hole site can be seen indirectly if they leave a characteristic imprint

on the subsequent Auger decay—i.e., if the decay of different core holes leads to significantly different charge and/or energy distributions in the doubly charged molecule.

The above-reported observations of the fragmentation pattern intensities suggested that the halogen and carbon core vacancies might result in clearly different final-state populations in the Auger decay. In order to investigate this possibility further, we carried out *ab initio* calculations of the molecular Auger spectra that, indeed, showed this to be the case. The calculations were then verified by a new AEPIPICO experiment.

Various degrees of sophistication can be applied to the *ab initio* calculations of molecular Auger spectra. In this paper, our goal is to compare the overall intensity distribution of the Auger electrons over the kinetic-energy range, following different core-hole decays, not to study the fine structure of the spectra. Therefore, a simple approach is applied where the Auger transition matrix elements are approximated using the atomic orbital contributions to the molecular orbitals, similar to Mitani *et al.* [38]. A single-configuration Hartree-Fock self-consistent field molecular orbital (MO) calculation was run for the neutral ground state using the GAMESS quantum chemistry code [39] and the 6-31G(d) basis set [40–43]. For each MO m, the total atomic orbital contribution from the atom k containing the core hole was calculated as

$$P_{m,k} = \sum_{i \in k} c_{m,i}^2, \tag{1}$$

where $c_{m,i}$ are the contribution coefficients from the atomic orbitals i belonging to the atom k that have higher energy than the core-hole orbital. Thus, for the chlorine $2p$ Auger decay, for example, for each MO the contribution from the chlorine orbitals $3s$ and $3p$ was calculated (in practice, the contribution of all the Gaussian basis set orbitals that were centered on chlorine and had higher energy than the Cl $2p_x$,$2p_y$, and $2p_z$ orbitals was calculated).

Next, all possible combinations of two MOs were performed representing the two final-state holes of the Auger decay with the criteria that the sum of the two orbital eigenenergies is higher than the orbital energy of the core hole:$\varepsilon_{m,n} = \varepsilon_m + \varepsilon_n > \varepsilon_{\mathrm{core},k}$. These combinations and their energy sums represent the Auger final states within Koopman's theorem approximation where the energy levels are given relative to the neutral ground state (see the sketch in Fig. 4). The intensities of the transitions filling the core-hole k and creating vacancies in the MO's m and n was then taken as proportional to the product,

$$I_{k,mn} \propto P_{m,k} P_{n,k}. \tag{2}$$

In order to generate a modeled spectrum comparable with the experiment, the "stick" spectrum for the decay of the core hole in atom k was convoluted with a Voigt function having 2.5-eV Gaussian and Lorentzian component widths. The result is shown in Fig. 5. Further complications will arise in the comparison with the experiment due to the presence of more than one energy level in the Auger initial (the core-hole) state. For Cl $2p$, these are due to the $2p$ spin-orbit splitting of about 1.7 eV so that the same final states are populated twice at different kinetic energies. To account for this, the modeled curve in Fig. 5 is a superposition of the two identical L_2VV and L_3VV spectra with the latter having been shifted by

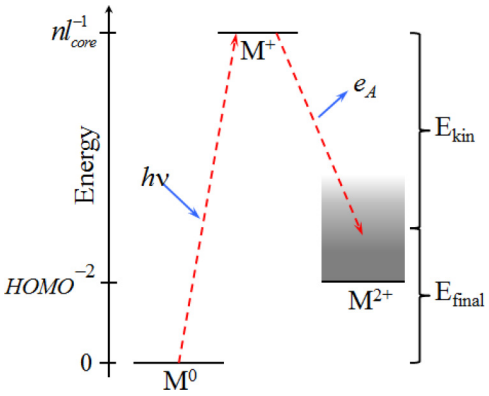

FIG. 4. (Color online) Schematic of the Auger process showing the correlation between the kinetic energy of the Auger electron and the internal energy of the doubly charged ion.

1.65 eV to the left. Note that this is only performed for a better comparability with the experiment presented later and should not be interpreted in terms of the internal final-state energy scale. Similarly, the experimental C KVV Auger spectrum will have inseparable contributions from both the C_{Cl} and the $C_{carboxyl}$ carbons. Their $1s$ binding energies differ by 2.77 eV due to the chemical shift (see Sec. III C), and therefore the $C_{carboxyl}$ $1s$ (which has the higher binding energy) KVV Auger electrons will have 2.77-eV higher kinetic energy than the C_{Cl} KVV Auger electrons. In order to again facilitate the comparability with the experiment, the Auger electron spectra from C_{Cl} and $C_{carboxyl}$ $1s$ holes (the dashed lines) were also combined into a single curve after shifting the $C_{carboxyl}$ spectrum by 2.77 eV.

As can be seen from Fig. 5, the calculations predict an essential difference in the way the various core-hole decays populate the dicationic states of the parent molecule $ClAA^{++}$: The low-energy final states in the Auger spectra receive much more intensity in the chlorine LVV Auger spectra than in either the C_{Cl} or the $C_{carboxyl}$ KVV Auger spectra. In the latter, the broad intensity maxima are centered around 30–40 eV of energy. Further investigation reveals that the origin of these

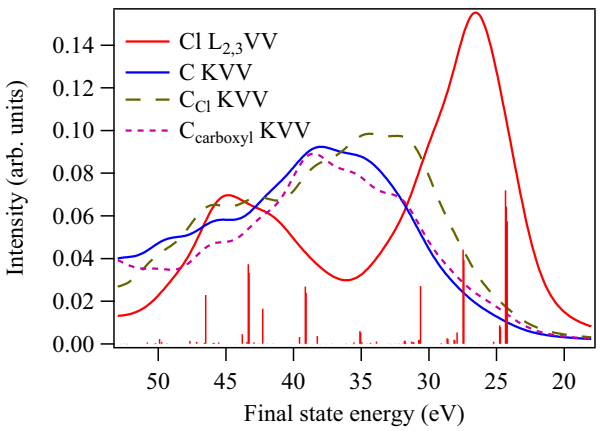

FIG. 5. (Color online) Modeled Auger electron spectra of ClAA for Cl $2p$ (the red curve) and C $1s$ (the blue curve) core-hole decays. The dashed lines show the contributions from the two carbons, and the vertical bars mark the intensities of individual final states in the Cl $L_{2,2}VV$ spectrum.

differences lies in the nature of the halogen valence orbitals $3p$. These orbitals make up the dominant contribution to the two outermost filled MOs. Consequently, the lower-energy Auger final states that involve these MOs have a large orbital overlap with the Cl $2p$ vacancy but very small overlaps with the C $1s$ vacancies, and thus the low-energy region of the C KLL spectra is suppressed.

An analogous calculation was performed for BrAA, and the result was very similar as for ClAA: a strong enhancement of the low-internal-energy portion of the spectrum for the decay of the $3d$ core hole in bromine as compared to the carbon $1s$ hole decay. Note that such an effect occurs specifically due to the halogen substitution since the valence electrons of the common light elements C, O, and N typically contribute more uniformly to the MO buildup of the organic molecules. Further scrutiny of the spectra in Fig. 5 shows that the Auger spectrum from the decay C $1s$ in the carboxyl group is more weighted towards higher final-state energies than the spectrum from C $1s$ adjacent to the halogen atom. This effect has also been observed for ethyl trifluoroacetate by Iwayama *et al.* [34] and is due to the so-called foreign imaging effect in Auger spectroscopy [34,44].

E. Auger decay spectra of core vacancies—experiment

In order to verify the theoretical prediction presented above, the noncoincident Auger electron spectra were measured (with the settings as in Table I) and are reported in Fig. 6. To facilitate the comparison with the modeled spectra in Fig. 5, the original kinetic-energy scale of the spectra in Fig. 6 was converted to a final-state energy scale by subtracting the kinetic energies from the average binding energies of C $1s$ and Cl $2p$ core levels, approximately 294.4 and 206.9 eV, respectively, obtained from separate photoelectron spectroscopy measurements. The Auger structure onsets in the experimental spectra appear at about 7-eV higher final-state energy than in the calculated spectra; this is expected since neutral ground-state orbital energies were used in the calculation of the double-hole configuration energies. Thus in the calculation, the removal of the second highest occupied molecular orbital electron requires as much energy as of the first one, whereas experimentally this energy is much larger due to orbital relaxation in the ionic state.

However, as in the calculated spectra of Fig. 5, the two experimental spectra now also provide a comparison of the overall intensity distribution of the Auger decay after ionizing different core-hole sites. The comparison fully confirms the theoretical prediction that the Cl LVV Auger strongly favors the low-energy final states. Although it is not our main purpose to represent the structure of the Auger spectra in detail by the calculations, comparing Figs. 5 and 6 displays a good agreement in this respect. The most notable discrepancy is the clear secondary maximum in the calculated Cl LVV spectrum at around 45-eV final-state energy. In the experimental spectrum, this corresponds to the final-state energy region around 50 eV, which does not show an increase in the intensity. However, the weak maximum around 46 eV is likely assigned to these final states as the energy shift is due to neglecting orbital relaxation in the calculations. Moreover, the discrepancies with the calculated intensities are as expected in such approximations [34,38].

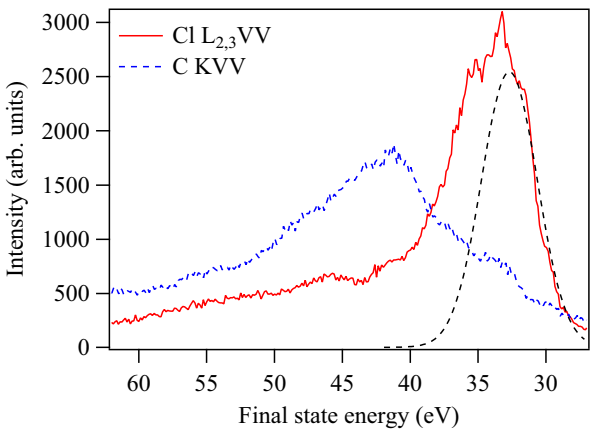

FIG. 6. (Color online) Measured noncoincident Auger electron spectra of ClAA for Cl $2p$ (the red curve) and C $1s$ (the blue dotted curve) core-hole decays. The dashed black curve indicates the instrument function used in the subsequent AEPIPICO measurement.

F. The effect of the internal energy—AEPIPICO measurements

The ion-ion mass spectra measured in coincidence with Auger electrons provide further evidence of the role of internal energy, and therefore the Cl LVV Auger spectrum in Fig. 6 was remeasured as an AEPIPICO experiment using photon energy of 250 eV. The electron energy resolution used in the AEPIPICO measurement was reduced as compared to the noncoincident spectra in Fig. 6 in order to obtain higher coincidence quality and sufficient energy range. The results of AEPIPICO measurements can be presented as (photo)ion -(photo)ion yield curves (PIPIYs) which show the number of coincidence events as a function of kinetic energy of the Auger electrons or alternatively as a function of final-state energy. The latter way of presentation was used here in order to facilitate the comparison with the spectra shown in the previous sections. In the production of PIPIY curves, false coincidence events were subtracted by using the ion-pair yields from the dataset with artificially generated triggers. However, such subtraction is approximate, and some contribution of the false coincidence background may remain. As an example of these yields, Fig. 7 presents the PIPIY curves of the pairs

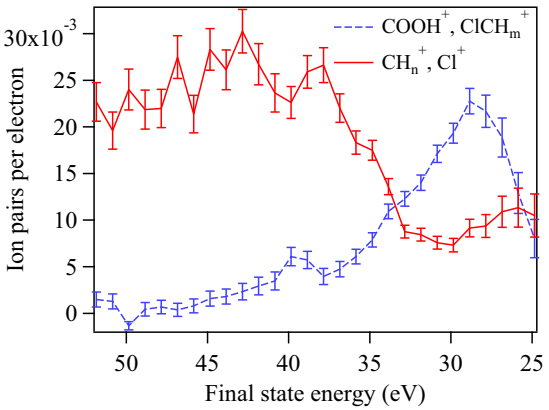

FIG. 7. (Color online) PIPIY curves of ion pairs (CH_n^+,Cl^+) and ($COOH^+$,$ClCH_m^+$).

(CH_n^+,Cl^+) and ($COOH^+$,$ClCH_m^+$) that showed a radical change in their intensities between different ionization sites (see Fig. 3). The PIPIY curves of those pairs also reveal a substantial difference: the maximum of the (CH_n^+,Cl^+) pair yield occurs at higher final-state energies compared with the ($COOH^+$,$ClCH_m^+$) pair. This is in agreement with the findings that the average internal energy of the molecule is larger after the C 1*s* core-hole decay and that the relative intensity of (CH_n^+,Cl^+) pairs increases in C 1*s* core ionization. The observation that the ($COOH^+$,$ClCH_m^+$) pairs are created in low-energy channels is also in accordance with the findings in PEPIPICO measurements (Fig. 3); based on the noncoincident Auger spectra in Figs. 5 and 6, the Cl 2*p* core-hole decay leads to a higher population of low-energy states than the C 1*s* core-hole decay, making this pair more abundant in Cl 2*p* ionization compared with C 1*s* ionization. These observations now also explain why one can observe an enhancement in halogen-ion separation when the halogen is in fact not the core-ionization site—if the halogen ion is produced in a high-energy dissociation channel, it is enhanced by the core-ionization leading, statistically, to more energetic doubly ionized states regardless of the initial localization of the core hole. And vice versa, the halogen bond is more likely to remain intact even following halogen ionization if the fragment in question [such as ($COOH^+$,$ClCH_m^+$)] belongs to a low-energy channel.

In order to reduce the information from PIPIY curves to just one parameter, we derived the average final-state energy corresponding to the Auger electrons detected in coincidence with the fragment pairs,

$$\bar{E}_{\text{state}} = \sum_n \frac{C^{\text{PIPIY}_n} E_{\text{state},n}}{C^{\text{PIPIY}_n}}. \quad (3)$$

Here the summation is over all data points n on the PIPIY curves. Next, the relative intensities of the fragment pairs observed in Cl 2*p* PEPIPICO measurements were divided by the relative intensities of the fragment pairs observed in C 1*s* PEPIPICO measurements. This ratio of relative intensities was then plotted vs $\bar{E}_{\text{state}}$ (Fig. 8). A clear rising trend can be observed from Fig. 8, which supports the notion that the pairs requiring more energy are less abundant in Cl 2*p* ionization.

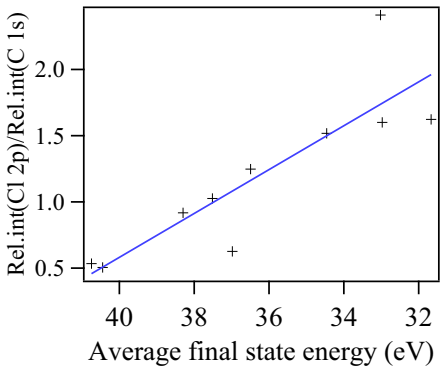

FIG. 8. (Color online) Intensity ratios of the observed fragmentation channels in PEPIPICO measurements (Fig. 3), the relative intensity of the fragment in Cl 2*p* ionization over the relative intensity in C 1*s* ionization, plotted vs the average final-state energy detected in coincidence with each channel. The straight line is a linear fit through the data points.

Lastly, also the slight tendency of the fragmentation pattern following C_x ionization sharing more similarities with the pattern following halogen ionization is well in line with the results of the calculated Auger intensities: For C_x they are biased towards smaller final-state energies.

IV. CONCLUSIONS

PEPIPICO spectroscopy measurements of core-ionized chloro- and bromoacetic acids revealed a noticeable site dependency in the photofragmentation in these molecules. Investigation of Auger spectra followed by C 1*s* and Cl 2*p* or Br 3*d* core-hole decay revealed a significantly different population of the final states in the internal energy of the doubly charged molecule. This explains the more extensive fragmentation of molecules after C 1*s* ionization. The AEPIPICO measurements of ClAA confirmed that the fragmentation indeed depended strongly on the internal energy of the molecule. Although the ionization site-dependent behavior was observed to be more pronounced in chloroacetic acid, similar effects were also seen in bromoacetic acid, which excludes the possibility of such a site-dependent effect being simply a sample-specific phenomenon.

In this study, we demonstrated another aspect of the ionization-site dependency of molecular dissociation following core-level photoabsorption. It arises as a consequence of the very common and strong effect of the internal energy dependency. Site dependency of this type does not manifest itself as the clear-cut "molecular knife" effect that was obtained in the site-selective core ionization in Ref. [26] but more as a statistical bias favoring dissociation channels with different internal energy requirements, depending on the core-ionization site. Interestingly, the effect of internal energy on the ion-pair yields was also observed in the study of core-excited 2Br pyrimidine [19]. In the studied molecules, site dependency is also not clearly linkable to the "local" character of the Auger process, although it was possible to do so for a bromochloromethane molecule [6]. We attribute this difference to the considerably more complex pattern of dissociation in the present molecule and the large role the carboxyl group plays in the dissociation dynamics.

According to the present study, it can be predicted that such site-dependent effects arise whenever the Auger decay of the various core holes populates the common final states with sufficiently different intensity distributions but does not require the core-ionization sites to be well separated spatially in the molecule. Therefore, in addition to considering the location of the core-ionization sites as in Refs. [25,26], it is of at least equal importance to consider the entire intensity distribution of the Auger decay and the criterion for site-dependency to occur. In Ref. [26], the criterion was that "*the atomic sites . . . should be located far from each other and connected through a chain of saturated bonds . . .*," which, in light of the present study, is not the only condition enabling site-dependent behavior.

Site-specific molecular-dynamics effects following molecular normal Auger decay are a more complex and multifaceted phenomenon than perhaps even realized in the first experiments. Recent advances in x-ray pump-probe experiments using free-electron lasers have already shown them to be excellent tools for investigating molecular dynamics, and that

they would also be very promising in further investigations of ionization-site-dependent fragmentation dynamics.

ACKNOWLEDGMENTS

We would like to acknowledge financial support from the Academy of Finland as well as the support by the European COST Action No. CM1204 XLIC. We would also like to thank the Electron Spectroscopy Group of the University of Oulu for sharing their experimental equipment for the PEPIPICO measurements of chloroacetic acid. The help of the staff of MAX Laboratory is much appreciated, and we especially thank the beamline post doc M.-H.Mikkelä for his kind assistance that exceeded the requirements of his duties.

[1] W. Eberhardt, T. K. Sham, R. Carr, S. Krummacher, M. Strongin, S. L. Weng, and D. Wesner, Phys. Rev. Lett. **50**, 1038 (1983).
[2] R. Murphy and W. Eberhardt, J. Chem. Phys. **89**, 4054 (1988).
[3] I. Nenner, C. Reynaud, H. C. Schmelz, L. Ferrand-Tanaka, M. Simon, and P. Morin, Z. Phys. Chem. **195**, 43 (1996).
[4] P. A. Hatherly, K. Codling, M. Stankiewicz, and M. Roper, J. Electron Spectrosc. Relat. Phenom. **79**, 407 (1996).
[5] A. P. Hitchcock, J. J. Neville, A. Jürgensen, and R. G. Cavell, J. Electron Spectrosc. Relat. Phenom. **88-91**, 71 (1998).
[6] C. Miron, M. Simon, N. Leclercq, D. L. Hansen, and P. Morin, Phys. Rev. Lett. **81**, 4104 (1998).
[7] T. Ibuki, K. Okada, K. Saito, and T. Gejo, J. Electron Spectrosc. Relat. Phenom. **107**, 39 (2000).
[8] X. J. Liu, G. Prümper, E. Kukk, R. Sankari, M. Hoshino, C. Makochekanwa, M. Kitajima, H. Tanaka, H. Yoshida, Y. Tamenori, and K. Ueda, Phys. Rev. A **72**, 042704 (2005).
[9] M. F. Erben, M. Geronés, R. M. Romano, and C. O. Della Védova, J. Phys. Chem. A **111**, 8062 (2007).
[10] A. Mocellin, K. Wiesner, S. L. Sorensen, C. Miron, K. L. Guen, D. Céolin, M. Simon, P. Morin, A. B. Machado, O. Björneholm, and A. N. de Brito, Chem. Phys. Lett. **435**, 214 (2007).
[11] A. Sugishima, K. Nagaya, H. Iwayama, M. Yao, J. Adachi, Y. Kimura, M. Yamazaki, and A. Yagishita, J. Chem. Phys. **131**, 114309 (2009).
[12] P. Salén, M. Kamińska, R. J. Squibb, R. Richter, M. Alagia, S. Stranges, P. van der Meulen, J. H. D. Eland, R. Feifel, and V. Zhaunerchyk, Phys. Chem. Chem. Phys. **16**, 15231 (2014).
[13] R. B. de Castilho, C. V. Nunez, A. F. Lago, A. C. F. Santos, L. H. Coutinho, C. A. Lucas, S. Pilling, M. O. Silva-Moraes, and G. G. B. de Souza, J. Electron Spectrosc. Relat. Phenom. **192**, 61 (2014).
[14] Y. Baba, Low Temp. Phys. **29**, 228 (2003).
[15] G. R. Chagas, V. S. V. Satyanarayana, F. Kessler, G. K. Belmonte, K. E. Gonsalves, and D. E. Weibel, ACS Appl. Mater. Interfaces **7**, 16348 (2015).
[16] W. Habenicht, H. Baiter, K. Müller-Dethlefs, and E. W. Schlag, J. Phys. Chem. **95**, 6774 (1991).
[17] S. Nagaoka, T. Fujibuchi, J. Ohshita, M. Ishikawa, and I. Koyano, Int. J. Mass Spectrom. Ion Processes **171**, 95 (1997).
[18] H. C. Schmelz, C. Reynaud, M. Simon, and I. Nenner, J. Chem. Phys. **101**, 3742 (1994).
[19] P. Bolognesi, J. A. Kettunen, A. Cartoni, R. Richter, S. Tosic, S. Maclot, P. Rousseau, R. Delaunay, and L. Avaldi, Phys. Chem. Chem. Phys. **17**, 24063 (2015).
[20] T. D. Thomas, L. J. Saethre, S. L. Sorensen, and S. Svensson, J. Chem. Phys. **109**, 1041 (1998).
[21] E. Itälä, D. T. Ha, K. Kooser, M. A. Huels, E. Rachlew, E. Nõmmiste, U. Joost, and E. Kukk, J. Electron Spectrosc. Relat. Phenom. **184**, 119 (2011).
[22] E. Itälä, K. Kooser, E. Rachlew, H. Levola, D. T. Ha, and E. Kukk, J. Chem. Phys. **142**, 194303 (2015).
[23] D. T. Ha, M. A. Huels, M. Huttula, S. Urpelainen, and E. Kukk, Phys. Rev. A **84**, 033419 (2011).
[24] E. Itälä, M. A. Huels, E. Rachlew, K. Kooser, T. Hägerth, and E. Kukk, J. Phys. B: At. Mol. Opt. Phys. **46**, 215102 (2013).
[25] S. Nagaoka, G. Prümper, H. Fukuzawa, M. Hino, M. Takemoto, Y. Tamenori, J. R. Harries, I. H. Suzuki, O. Takahashi, K. Okada, K. Tabayashi, X.-J. Liu, T. Lischke, and K. Ueda, Phys. Rev. A **75**, 020502 (2007).
[26] S. Nagaoka, H. Fukuzawa, G. Prümper, M. Takemoto, O. Takahashi, K. Yamaguchi, T. Kakiuchi, K. Tabayashi, I. H. Suzuki, J. R. Harries, Y. Tamenori, and K. Ueda, J. Phys. Chem. A **115**, 8822 (2011).
[27] J. H. D. Eland, P. Linusson, M. Mucke, and R. Feifel, Chem. Phys. Lett. **548**, 90 (2012).
[28] K. Müller-Dethlefs, M. Sander, L. A. Chewter, and E. W. Schlag, J. Phys. Chem. **88**, 6098 (1984).
[29] M. Hoener, D. Rolles, A. Aguilar, R. C. Bilodeau, D. Esteves, P. Olalde Velasco, Z. D. Pešić, E. Red, and N. Berrah, Phys. Rev. A **81**, 021201 (2010).
[30] J. Laksman, K. Kooser, H. Levola, E. Itälä, D. T. Ha, E. Rachlew, and E. Kukk, J. Phys. Chem. B **118**, 11688 (2014).
[31] P. A. Hatherly, K. Codling, M. Stankiewicz, and M. Roper, J. Phys. B: At. Mol. Opt. Phys. **28**, 3249 (1995).
[32] E. Kukk, D. T. Ha, Y. Wang, D. G. Piekarski, S. Diaz-Tendero, K. Kooser, E. Itälä, H. Levola, M. Alcamí, E. Rachlew, and F. Martín, Phys. Rev. A **91**, 043417 (2015).
[33] K. Ueda, J. Electron Spectrosc. Relat. Phenom. **141** (2004).
[34] H. Iwayama, N. Sisourat, P. Lablanquie, F. Penent, J. Palaudoux, L. Andric, J. H. D. Eland, K. Bučar, M. Žitnik, Y. Velkov, Y. Hikosaka, M. Nakano, and E. Shigemasa, J. Chem. Phys. **138**, 024306 (2013).
[35] E. Kukk, R. Sankari, M. Huttula, A. Sankari, H. Aksela, and S. Aksela, J. Electron Spectrosc. Relat. Phenom. **155**, 141 (2007).
[36] M. Bässler, J. Forsell, and O. Björneholm, J. Electron Spectrosc. Relat. Pheom. **103**, 953 (1999).
[37] E. Itälä, D. T. Ha, K. Kooser, E. Nõmmiste, U. Joost, and E. Kukk, Int. J. Mass Spectrom. **306**, 82 (2011).
[38] M. Mitani, O. Takahashi, K. Saito, and S. Iwata, J. Electron Spectrosc. Relat. Phenom. **128**, 103 (2003).
[39] M. W. Schmidt, K. K. Baldridge, J. A. Boatz, S. T. Elbert, M. S. Gordon, J. H. Jensen, S. Koseki, N. Matsunaga, K. A. Nguyen, S. Su, T. L. Windus, M. Dupuis, and J. A. Montgomery, J. Comput. Chem. **14**, 1347 (1993).
[40] R. Ditchfield, W. J. Hehre, and J. A. Pople, J. Chem. Phys. **54**, 724 (1971).

[41] W. J. Hehre, R. Ditchfield, and J. A. Pople, J. Chem. Phys. **56**, 2257 (1972).

[42] M. M. Francl, W. J. Pietro, W. J. Hehre, J. S. Binkley, M. S. Gordon, D. J. DeFrees, and J. A. Pople, J. Chem. Phys. **77**, 3654 (1982).

[43] P. C. Hariharan and J. A. Pople, Theor. Chim. Acta **28**, 213 (1973).

[44] F. O. Gottfried, L. S. Cederbaum, and F. Tarantelli, J. Chem. Phys. **104**, 9754 (1996).